Multi-Domain Seismic Noise Reduction in 2D Land Data: A Case Study from Poland

BABAN MUSTAFA YOUSEF

Dept. of Geology, College of Science, University of Duhok, Kurdistan Region–Iraq

Corresponding authors Email: baban.yousef@uod.ac

Abstract:

Seismic reflection data are often contaminated by various types of noise, particularly ground-roll, which can obscure true reflection signals and hinder data interpretation. Effective noise reduction is essential for improving the signal-to-noise ratio and revealing subsurface structures. Many noise suppression techniques rely on transforming seismic data into different domains, making it easier to separate noise from useful signals. In this study, we applied a range of algorithms across multiple domains—including shot, receiver, t-x, f-x, f-k, R-T, and offset class domains to effectively reduce both coherent and random noise in 2D seismic land data. Our results demonstrate that these multi-domain filtering methods significantly enhance seismic image quality, enabling clearer and more reliable structural and stratigraphic analysis.

Keywords: Seismic Reflection, 2D survey, Processing, Migration, Pre-stack time migration (PSTM), Post-stack time migration (POSTM).

1. Introduction

Seismic data processing plays a vital role in both exploration geophysics and broader geophysical studies, with its practical value demonstrated through the analysis of real datasets and instructional case studies (Yilmaz, 2001; Sheriff & Geldart, 1995). By exploring the fundamental physics and mathematical principles behind various seismic analysis techniques, students and practitioners gain insight into both the capabilities and limitations of these methods for modelling subsurface structures (Kearey et al., 2013).

Seismic datasets are often contaminated by noise, which must be minimised to improve the signal-to-noise ratio (SNR) and enhance data quality (Chen & Ma, 2014). In the context of seismic exploration, noise refers to any component of the recorded signal that is uninterpretable or unwanted, arising from a variety of sources (Stewart, 1984). While some of these unwanted events may resemble useful signals, they typically provide misleading or insufficient information about the subsurface. Such noise is generally classified as either random or coherent (Yilmaz, 2001).

Seismic noise encompasses all extraneous energy captured during data acquisition that interferes with the interpretation of seismic signals. Any recorded energy that does not align with the expected seismic response is considered noise, which can manifest as either random fluctuations or coherent patterns (Sheriff & Geldart, 1995). The distinction between signal and noise is based on whether the recorded energy conforms to the conceptual model of the seismic event under investigation (Kearey et al., 2013).

Multiple seismic events, such as those that have undergone more than one reflection within the subsurface, further complicate the interpretation process (Yilmaz, 2001). The signal-to-noise ratio (SNR) serves as a key metric for assessing the quality of seismic data, representing the relative strength of the desired signal compared to background noise (Canales, 1984).

Seismic data can be acquired using both active and passive methods. Active seismic surveys employ artificial sources, such as dynamite or vibroseis for land studies and air guns for marine environments, and are commonly used in exploration and engineering seismology. In contrast, passive seismic methods rely on natural sources, including earthquakes, solar activity, and ocean waves, and are typically applied in earthquake seismology (Kearey et al., 2013).

Noise in seismic data is typically divided into two main categories: random (incoherent) noise and coherent noise. Coherent noise is characterised by its organised, repetitive, or predictable patterns, which can often be traced across multiple seismic traces. This type of noise is systematic and can be identified due to its consistency across the dataset (Yilmaz, 2001). In contrast, incoherent (random) noise varies from trace to trace and lacks any predictable pattern, making it impossible to anticipate its appearance based on adjacent traces. Random noise is commonly generated by external factors such as human activity, animals, or environmental conditions like wind (Sheriff & Geldart, 1995).

Strong coherent noise, such as ground roll, has long posed challenges in seismic data processing by degrading data quality (Stewart, 1984). Over the years, various techniques have been developed to suppress or eliminate such noise during both the data acquisition and processing stages (Ulrych et al., 1995). Despite these efforts, coherent noise remains a persistent issue in seismic datasets. Bandpass filters are frequently employed to reduce ground roll noise, as this type of noise predominantly occupies the low-frequency range, where little valuable signal is present (Yilmaz, 2001).

Time-variant spectral whitening (TVSW) is another effective technique for attenuating ground roll noise. TVSW works by decomposing each seismic trace into multiple frequency sub-bands, then scaling these sub-bands in a time-dependent manner to achieve a uniform amplitude level. The final output is obtained by summing the scaled sub-band traces. According to Perz et al. (2005), TVSW offers several advantages, including compensation for high-frequency attenuation over time (due to Q), balancing the amplitude spectrum outside the deconvolution design window, and effective noise reduction. The method suppresses ground roll by reducing its high amplitude at low frequencies to match the average signal spectrum across the bandwidth.

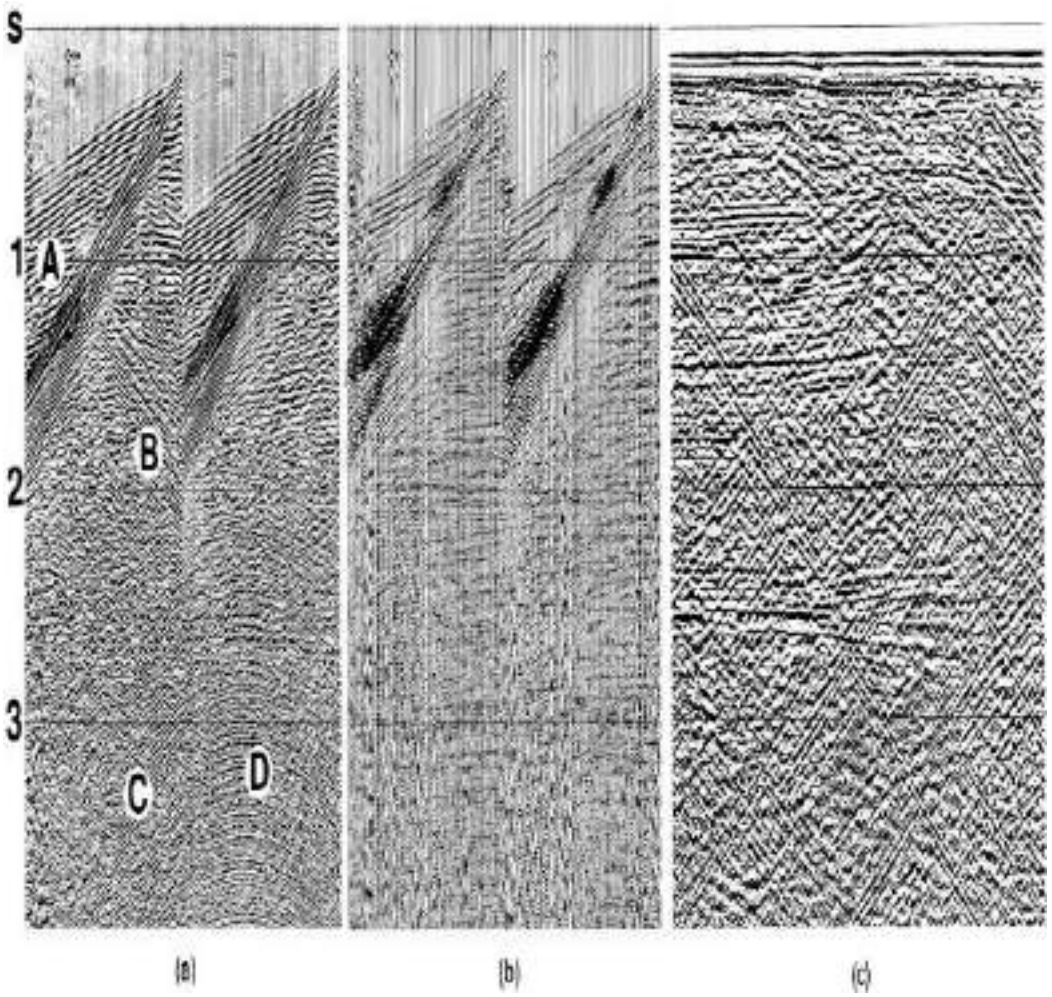

Figure (1) (a) Two common-shot gathers and (b) two CMP gathers from the same line; (c) CMP stack. (Data courtesy Taylor Woodrow Energy Ltd.). From seismic data analysis Yilmaz (2001).

2. Materials and Methods

2.2. Data used and processing software

In this research, a single line of two-dimensional raw seismic reflection data from Poland, supplied by the Society of Exploration Geophysicists (SEG) in SEG-Y file format, was utilised. The data underwent comprehensive processing using a system designed for handling large-scale marine or terrestrial seismic surveys, accommodating both 2D and 3D datasets, as well as pre-stack and post-stack information. This system employs advanced geophysical algorithms, analytical tools, and optimised parallel processing capabilities to efficiently manage and process substantial data volumes (Landmark, 2013). The software runs on a Linux platform and features a flow editor, which allows users to construct processing sequences by selecting appropriate modules from the "Process list." This list encompasses essential processing steps such as "Geometry/Headers," "Editing/Muting/Noise," and "Data Input/Output," along with various subsections within these categories (Reiner, 2018). The processing workflow adopted in this study is illustrated in Figure.

An energy source generates elastic waves that travel through the subsurface, and these waves are detected by a seismograph using arrays of geophones or hydrophones. The velocity and trajectory of these waves are influenced by the ground's density, elasticity, and structural

composition. By capturing the wave movements with seismic instruments and analysing their characteristics and travel times, it is possible to construct a model of the subsurface geology. The seismic velocities measured for different layers provide valuable information about the type of material present, as well as its mechanical strength and stability higher velocities generally correspond to more competent or stable materials. The specific type of motion recorded depends on the equipment and survey methodology employed. Common seismic survey techniques include refraction, reflection, surface wave, and borehole methods. SeisSpace ProMAX® software offers advanced algorithms for both prestack and poststack time and depth imaging. Additionally, its integrated development kit allows users to incorporate custom processing algorithms, enabling the creation of tailored workflows within the ProMAX® environment.

3. Results and Discussion

3.1. Coherent linear noise:

Two types of coherent linear noise that deserve special attention are guided waves and side-scattered energy.

Figure 1 displays field data that reveal coherent linear noise patterns across three domains: the common-shot gather, the common-midpoint (CMP) gather, and the CMP stack. In Figure 6.0-1a, the dispersive waves labelled as A are recognised as guided waves, while the linear features marked B and C, along with the curved events denoted as D, are associated with side scatterers. Guided waves manifest as dispersive linear noise in both the common-shot and CMP gathers; however, their influence is greatly diminished after stacking.

These guided waves are usually restricted to a water layer or a shallow, low-velocity zone near the surface, travelling predominantly in a horizontal direction. Their dispersive nature means that different frequency components move at varying phase velocities, a phenomenon best explained by normal-mode propagation theory. Theoretical and numerical modelling of guided waves using this approach has been explored in previous studies. Because guided waves do not contain valuable reflection information, they are typically suppressed or muted in CMP gathers. However, if a particular mode separates from the main guided wave packet and travels at a lower velocity, thereby overlapping with reflection events, frequency-wavenumber (f-k) domain dip filtering becomes necessary to suppress this interference. A clear example of guided waves can be observed in the field record, particularly between 1 and 4.5 seconds at far offsets.

As shown in Figure 2, the early portion of the wave packet visible between 1 and 1.5 seconds at far offset is primarily composed of low-frequency energy. High-frequency signals follow the direct arrival path, appearing around 0.3 seconds at near offset and extending to about 1.8 seconds at far offset, while mid-range frequencies are observed between 1.8 and 2.8 seconds at far offset. A distinct, very low-frequency, high-amplitude dispersed wavetrain, occurring between 2.8 and 4.5 seconds at far offset, represents a mode that has diverged from the main group of guided-wave modes. This separation is commonly found in regions with a shallow, soft seabed, often linked to the presence of a mud layer.

The data also reveal a backscattered guided wave (zone B) characterised by a reverse linear moveout, indicating irregularities on the seafloor. These seafloor features also produce arrivals in zone A, which are associated with point scatterers.

The dispersive properties of guided waves can change along the seismic profile, depending on variations in water depth and the characteristics of the water-bottom boundary. Typically, shallower water and softer seabed conditions increase both the dispersion and the splitting of guided wave modes.

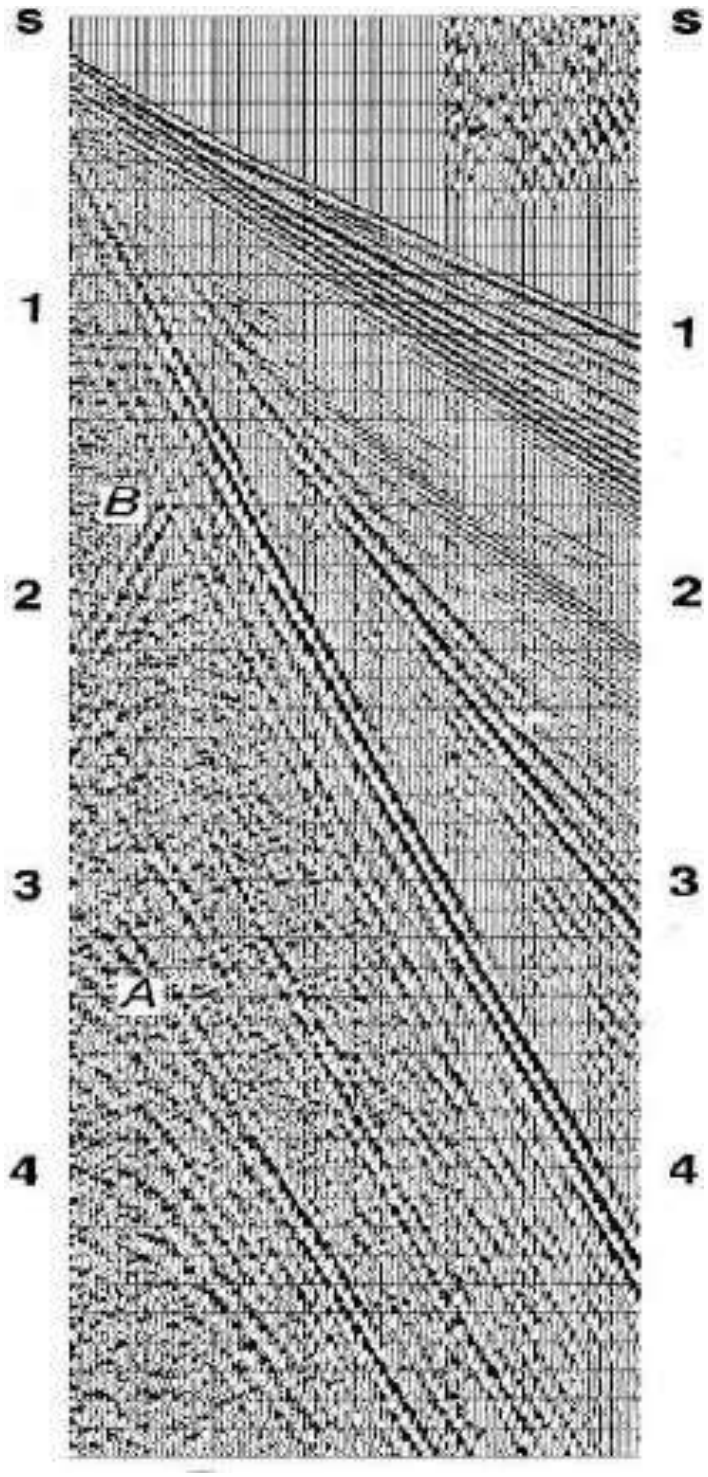

Figure (2) A shot gather containing predominantly guided waves. From seismic data analysis Yilmaz, (2001).

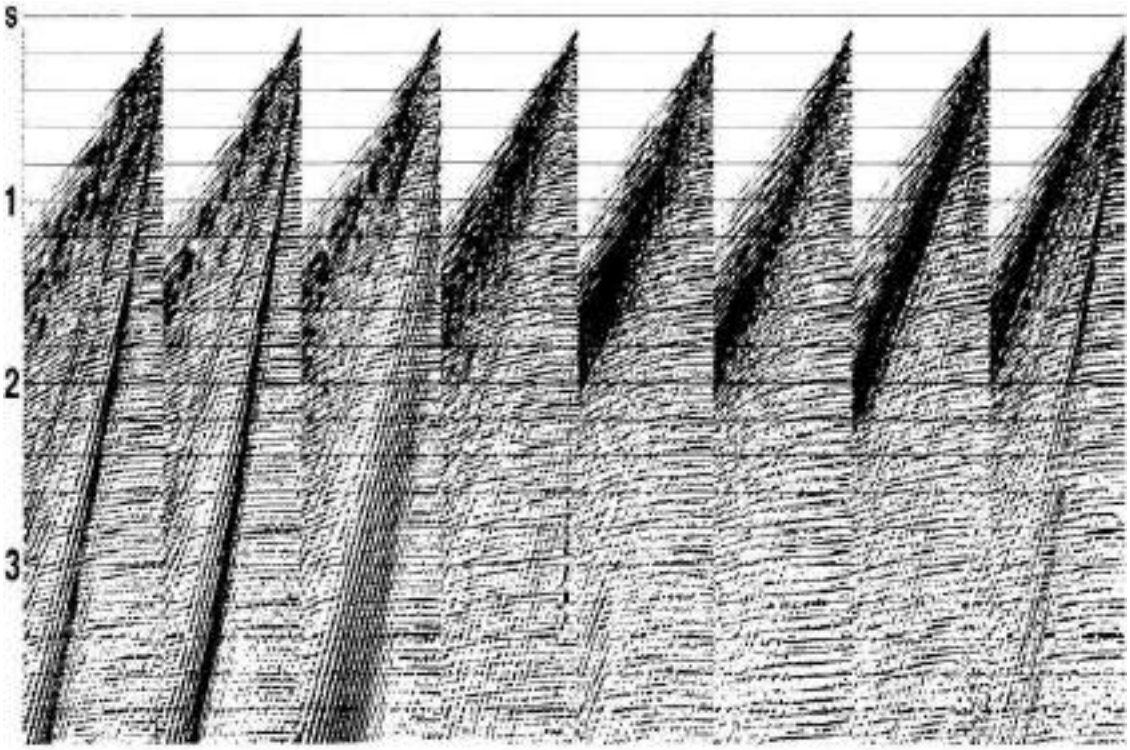

Figure (3) Shot gathers containing guided waves with varying strength, reverberations and short-period multiples Yilmaz, 2001.

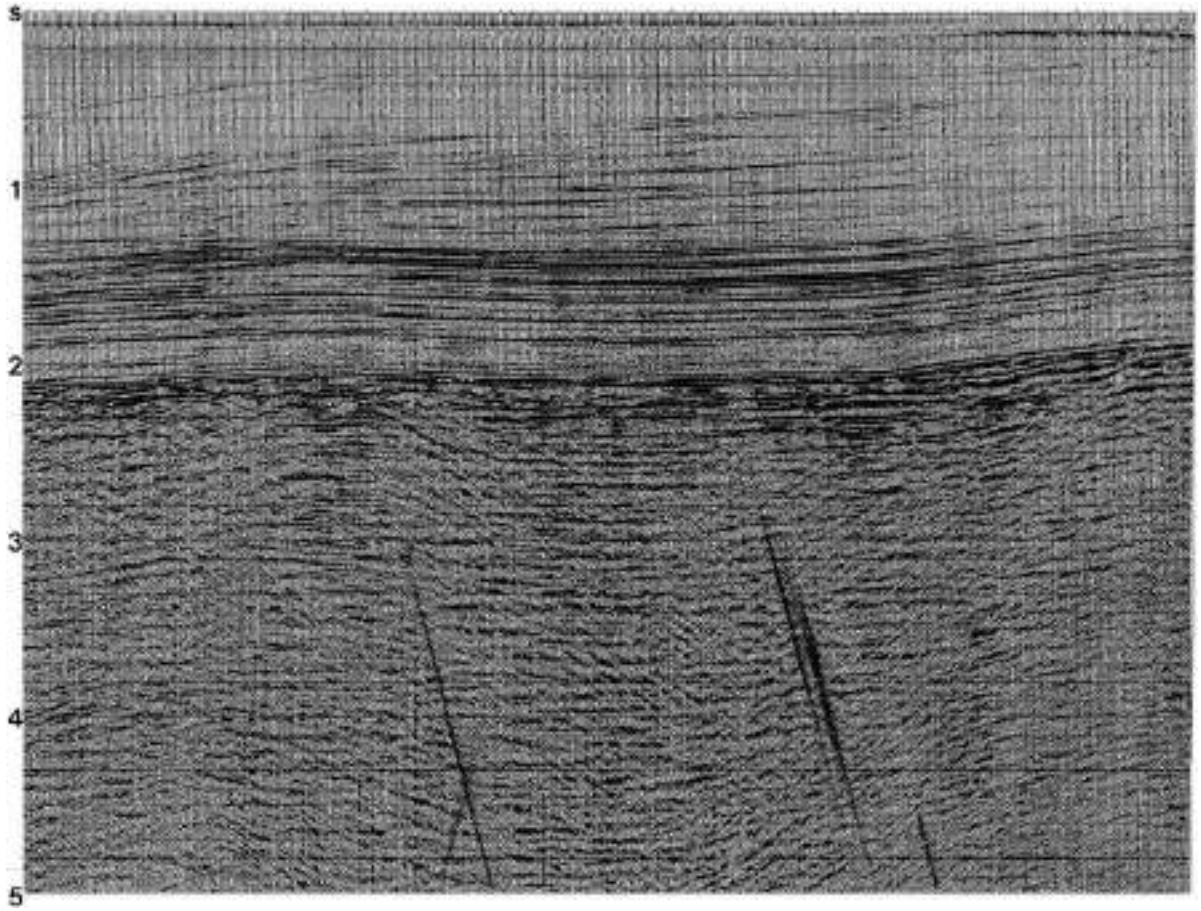

Figure (4). A CMP stack that contains diffraction energy associated with side scatterers at the water bottom. From seismic data analysis, Yilmaz (2001).

Side-scattered energy exhibits a wide range of moveouts, which depend on the relative position of the scatterer acting as a point source at the water bottom to the location of the recording cable (as illustrated by events B, C, and D in Figure 1a). On common-shot gathers (Figure 1a), side-scattered energy appears with variable moveout, but it is generally absent in common-midpoint (CMP) gathers (Figure 1b). However, this energy re-emerges as linear noise in stacked sections (Figure 1c) (Larner et al., 1983). Side-scattered energy tends to stack at high velocities along the linear portions of its travel time curve. Consequently, the linear noise observed in stacked sections, especially at later times, is most likely due to scattered energy along the flanks of its travel time curve, which is stacked together with high-velocity primary reflections (see Figure 4).

Linear noise associated with side scatterers is recognised easily on a time scale from a 3-D volume of stacked data. Note in Figure 6.0-5 the circular patterns expanding out from the source of a series of point scatterers at the water bottom. In this case, certain parts of the sea- bottom pipelines act as point scatterers.

Figure (5): presents a time slice extracted from an unmigrated 3-D stacked data volume, displaying circular features that are linked to point scatterers located along sea-bottom pipelines. (Data provided by Total Argentina; adapted from Yilmaz, 2001).

In this setting, sections of sea-bottom pipelines may act as point scatterers. Several methods can be employed to reduce the coherent linear noise produced by these side scatterers, such as frequency-wavenumber (f–k) filtering, the τ–p (slant-stack) transform, and the Radon transform. In the f–k domain, linear features on shot records appear as radial lines, which can be effectively attenuated using f–k dip filters. Likewise, in the τ–p domain, linear events are transformed into points, enabling their suppression through muting. Additionally, when mapping CMP gathers to the Radon-transform domain—which relies on hyperbolic moveout—both spatially random and coherent linear noise are largely excluded. As a result, the CMP gathers reconstructed via the inverse Radon transform are largely free from these types of noise.

Coherent linear noise is also a common issue in land seismic surveys, where it often appears as dispersive Rayleigh waves, or ground roll. This noise is characterised by its low group velocity, high amplitude, and dominance at low frequencies. As shown in Figure 6, ground-roll energy is most prominent in traces recorded at near offsets.

Reflections generally become visible only after amplitude scaling has been applied. As shown in the selected shot records in Figure 6, both the intensity and apparent dip (stepout) of the dispersive waves linked to ground-roll energy fluctuate in response to variations in near-surface conditions. Swell noise is observed on shot records as low-frequency vertical bands (refer to Figure 7). This type of noise is typically caused by rough sea states during marine seismic data acquisition, especially in shallow water areas. Employing a low-cut filter is often an effective method for reducing swell noise in shot records

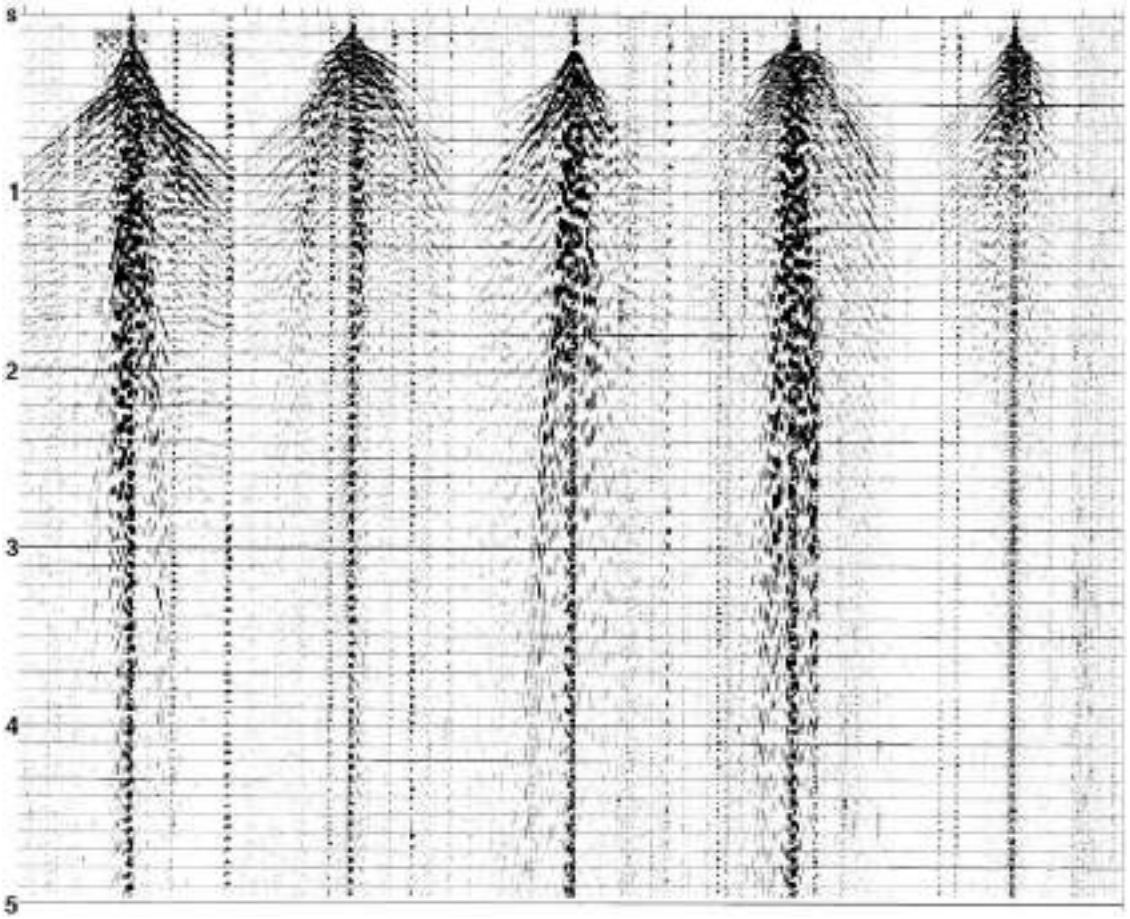

Figure (6): Sample shot records from a 2-D land seismic line are presented. Ground-roll energy

is much more prominent than any potential reflection signals within the data. The red triangle highlights the presence of ground roll in the gather (adapted from Yilmaz, 2001).
Swell noise is visible on shot records as vertical bands of low-frequency energy (refer to Figure 8). This type of noise is usually produced by turbulent sea conditions during marine seismic surveys, especially in shallow water environments. Applying a low-cut filter is a standard and effective approach for reducing swell noise in shot records.

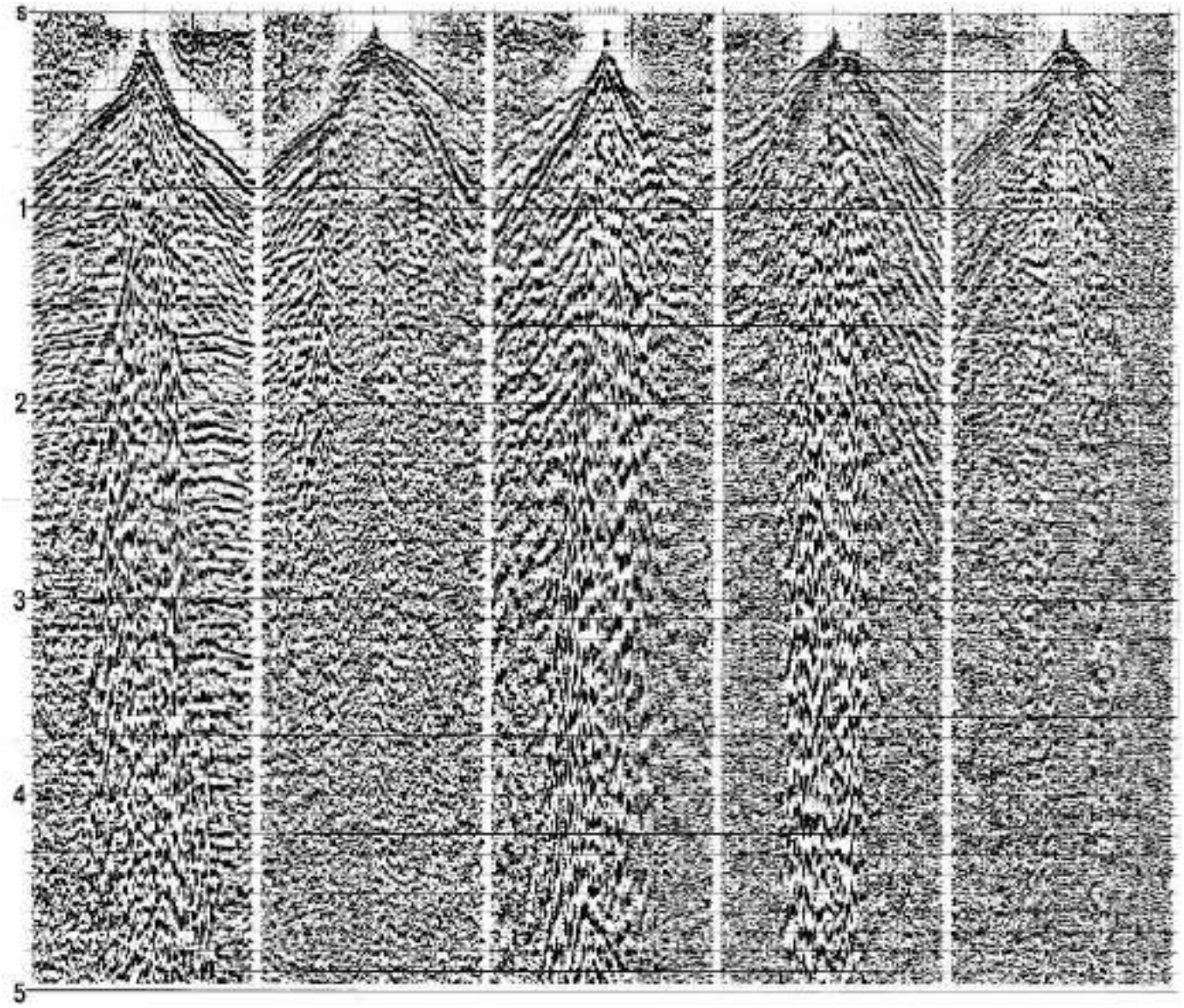

Figure (7): The records displayed in Figure (5) are shown again here, but with automatic gain control (AGC) applied to improve the visibility of reflection energy, which is otherwise masked by strong ground-roll energy. (Adapted from data analysis by Yilmaz, 2001).

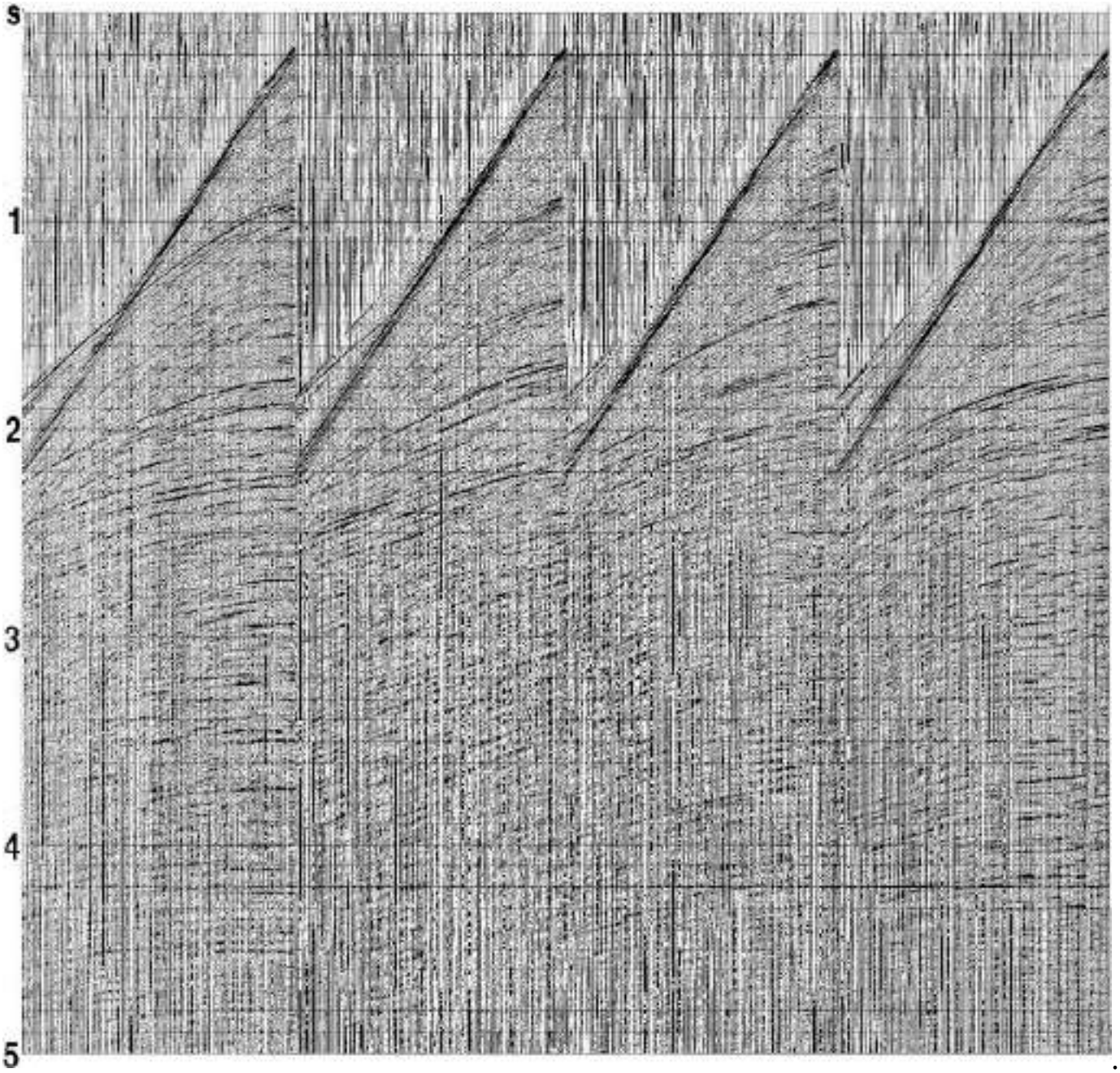

Figure (8): Selected shot records from a marine 2-D line with swell noise. From seismic data analysis Yilmaz, (2001).

Another form of coherent noise, known as cable noise, is characterised by low-frequency linear events with pronounced stepout, as illustrated in the shot records in Figure 8. The intensity of cable noise tends to increase as the water depth decreases. Similar to swell noise, cable noise can often be effectively attenuated from shot records using a low-cut filter.

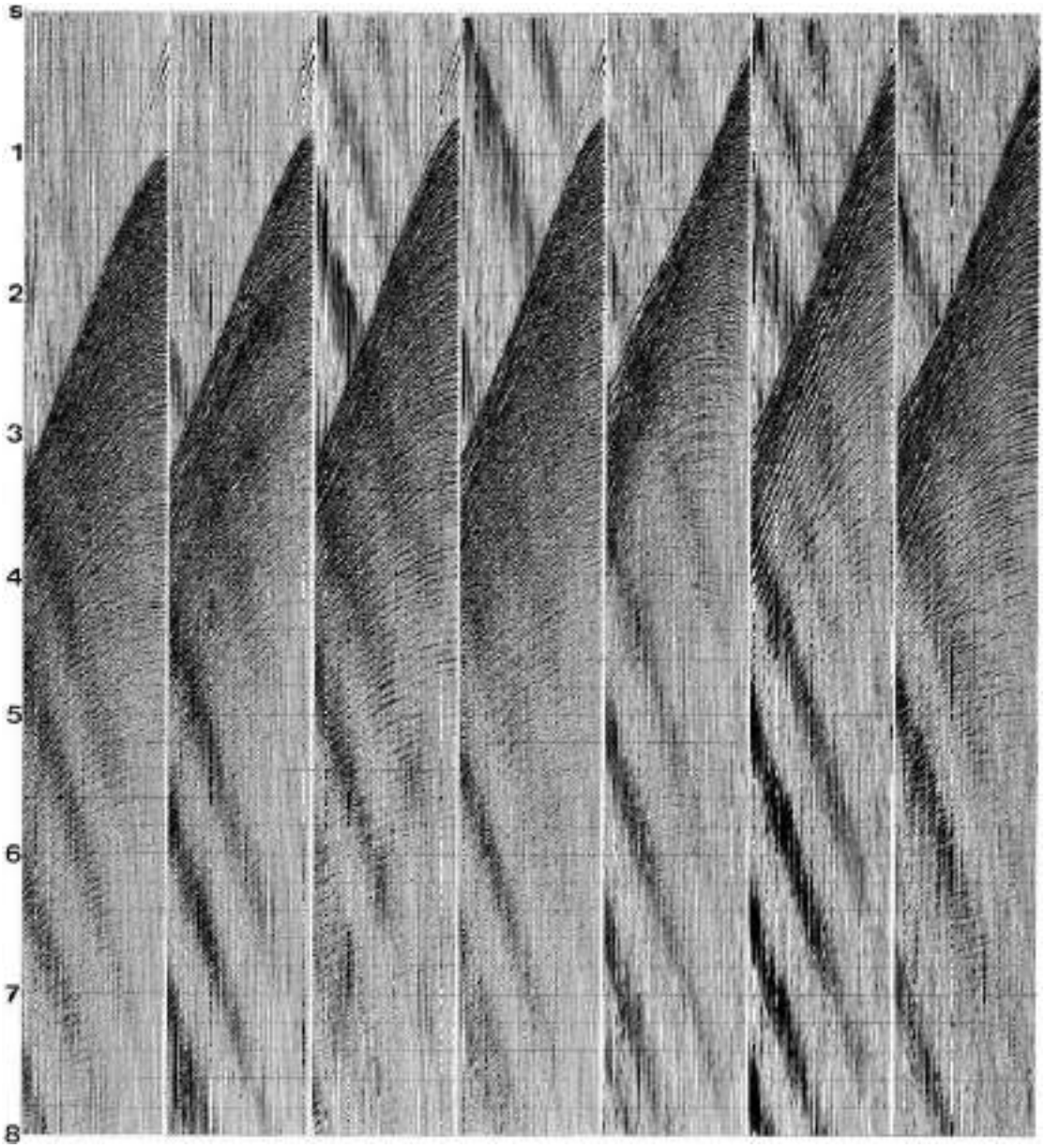

Figure (9): Example shot records from a marine 2-D seismic line exhibiting swell noise. (Adapted from seismic data analysis by Yilmaz, 2001).

3.2. Surface Consistent Amplitudes (SCA)

Surface Consistent Amplitudes is a process designed to estimate and correct for the relative amplitude contributions of sources, receivers, offset bins, CDPs, and channels in a manner that is consistent across the acquisition surface. The amplitude recorded on any given seismic trace is influenced by several factors, including the energy of the source, the response and coupling efficiency of the receivers, the characteristics of the amplifier channel, the trace offset, and the physical properties of the subsurface reflectors, as well as less quantifiable influences such as ambient noise. While it is challenging to isolate these effects on an individual trace, statistical analysis across multiple traces allows for their estimation. For instance, traces associated with a particularly weak source will generally exhibit lower amplitudes, while those recorded at a specific receiver location may display higher amplitudes due to superior geophone coupling. Similarly, certain channels may deviate from the average response. It is important to note that

CDP, offset bin, and channel are typically not considered surface-consistent domains. The Surface Consistent Amplitudes process is typically implemented in three stages: Input, Compute, and Apply.

3.3. Input mode

This is the first pass. It estimates the amplitude for each input trace over a specified time gate and writes the amplitude to the TRC database. Amplitude is estimated in a time gate. One and only one-time gate per trace must be specified, but the gate may vary spatially along the line. If the time gate for a trace is less than the minimum threshold length, parameter Minimum gate width, the program resets the gate to the minimum length. The reset time gate is centered on the starting time of the original gate. The program can compute statistical amplitude estimates by the following methods:

1. Use the mean of the absolute amplitude of all nonzero samples in the gate.

2. Use the RMS of all nonzero samples in the gate.

3. Use the median of a set of mean amplitudes computed for 21 subgates of the instantaneous amplitude envelope trace. Here is what happens for this option:

• Compute the instantaneous amplitude envelope trace using a Hilbert transform.

• Divide the gate into 21 expanding subgates. Subgate 1 contains the first 1/21 samples of the gate, subgate 2 the first 2/21 samples, and so on.

• Compute the mean of the amplitude envelope of all nonzero samples in each subgate.

• Use the median of the 21 subgate amplitudes as the value for this trace. Only subgates containing nonzero values are used to derive the median.

3.4. True Amplitude Recovery (TAR)

True Amplitude Recovery applies a gain function—potentially varying in both time and space—to seismic traces to compensate for amplitude losses resulting from wavefront spreading and attenuation. In ProMax® VSP, this process is referred to as VSP True Amplitude Recovery, with some differences in its implementation. The procedure provides several amplitude recovery methods, which can be applied individually or in combination. These options include corrections for spherical divergence, inelastic attenuation, decibel-per-second (dB/sec) adjustments, and power-of-time corrections. At least one of these correction methods must be selected for the process to proceed.

3.5. Spherical divergence correction

This correction compensates for loss of amplitudes due to spherical wavefront spreading. If $(\frac{1}{dist})$ for **Basis for spherical spreading**, the gain correction is

$$g(t) = t \times v(t)$$

If $1/(time \times vel^2)$ for **Basis for spherical spreading**, the gain correction is

$$g(t) = t \times v^2(t)$$

where *t* is time and *v(t)* is an RMS (stacking) velocity function.

3.6. Inelastic attenuation correction

This correction compensates for loss of amplitudes due to inelastic attenuation. The gain correction is:

$$g(t) = e^{\propto \times t \times v(t)}$$

Where ∝ is the inelastic attenuation correction constant, *t* is time and *v(t)* are an RMS (stacking) velocity function.

3.7. SEG-Y Input

SEG-Y Input reads data from tapes approximately conforming to the SEG-Y to display a shot, gather. this is the shot gather:

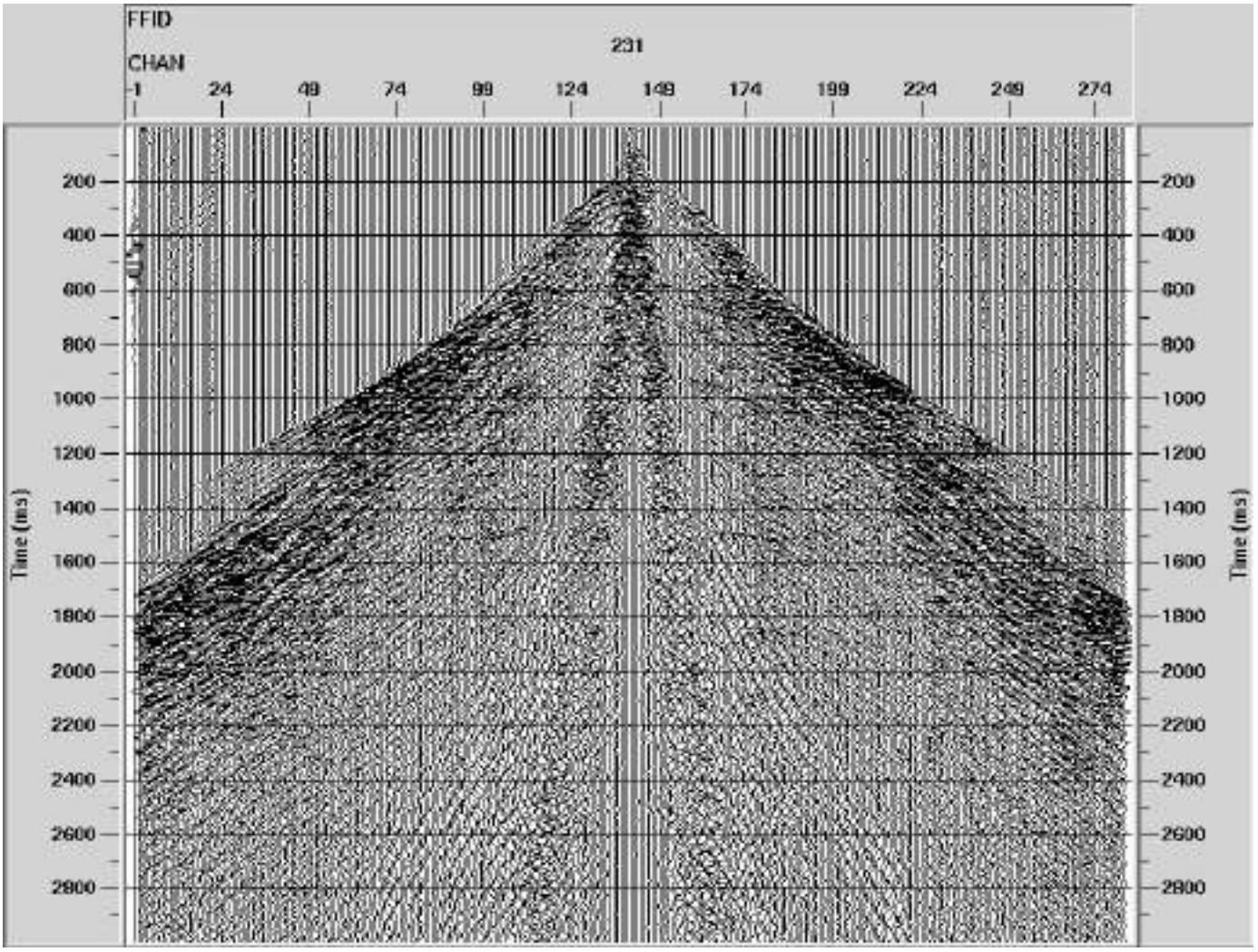

Figure 10: The shot gathers before applying geometry

One way to determine if geometry has been correctly applied to the shot gather is by observing the presence of a flagged mark along the channel axis (indicated by a red circle). A technique often employed to verify the accuracy of the geometry is by performing a Brute stack.

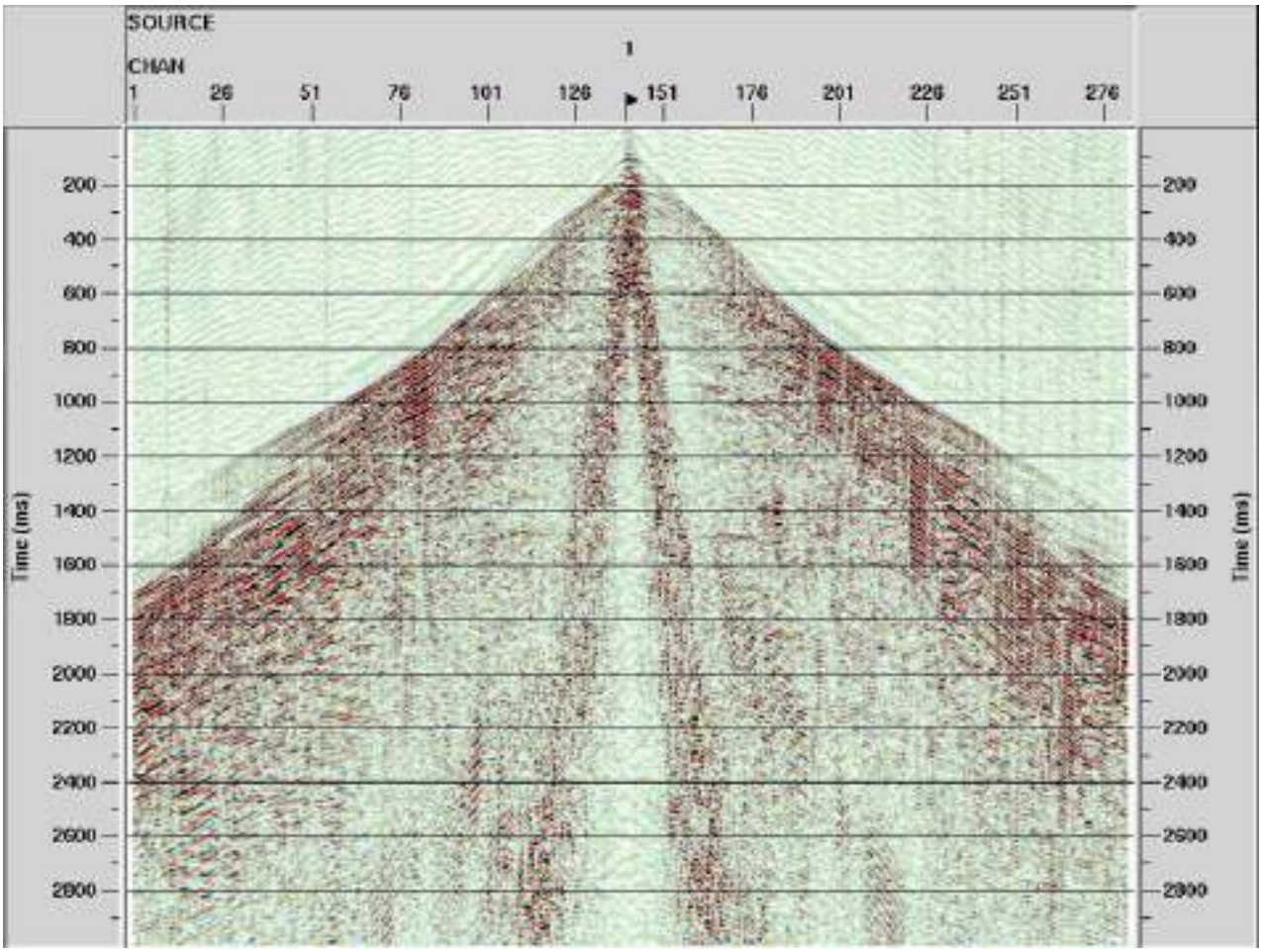

Figure 11: The shot gathers after applying geometry for source 1.

Table 1: Picking Hyperbolics.

No.	T_0 (ms)	Velocity (m/s)
1	270	1400
2	570	2400
3	900	2200
4	1100	2500
5	1470	2900
6	1800	2800

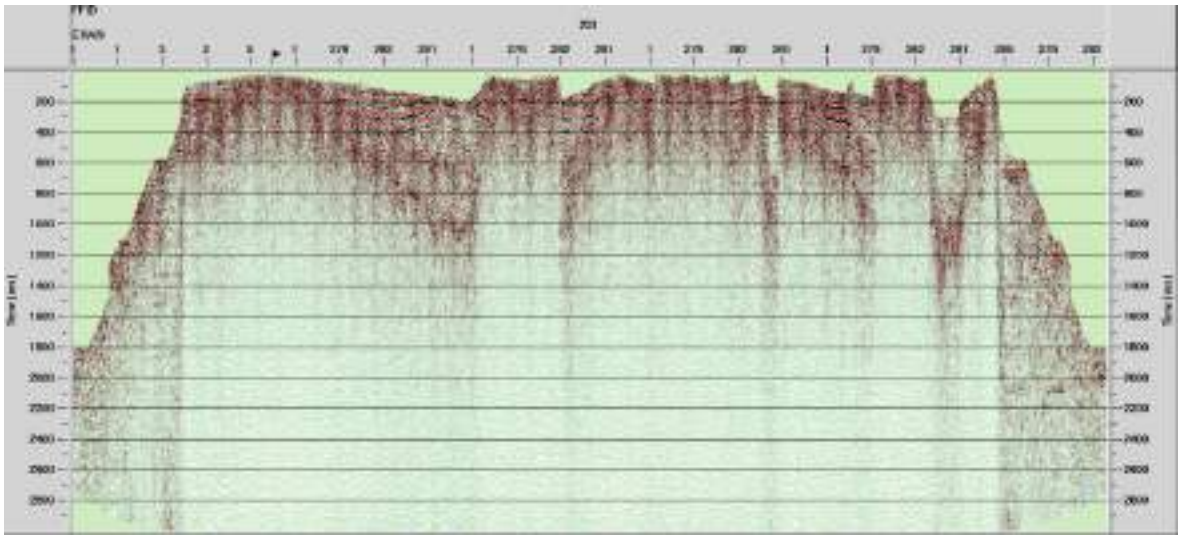

Figure 12: Brute stack with stretch muting 0%.

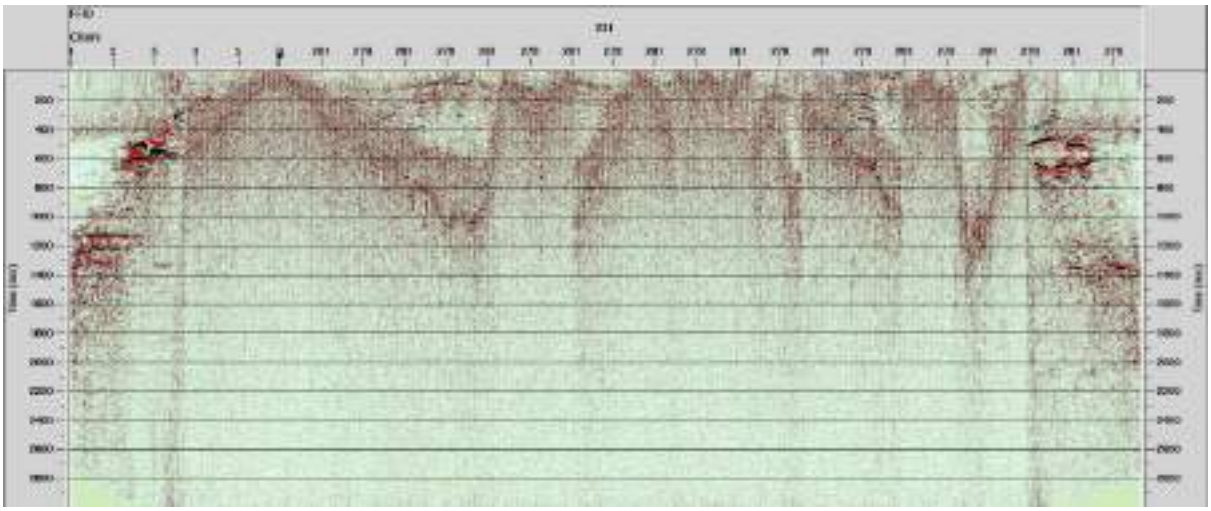

Figure 13: Brute stack with stretch muting 30%.

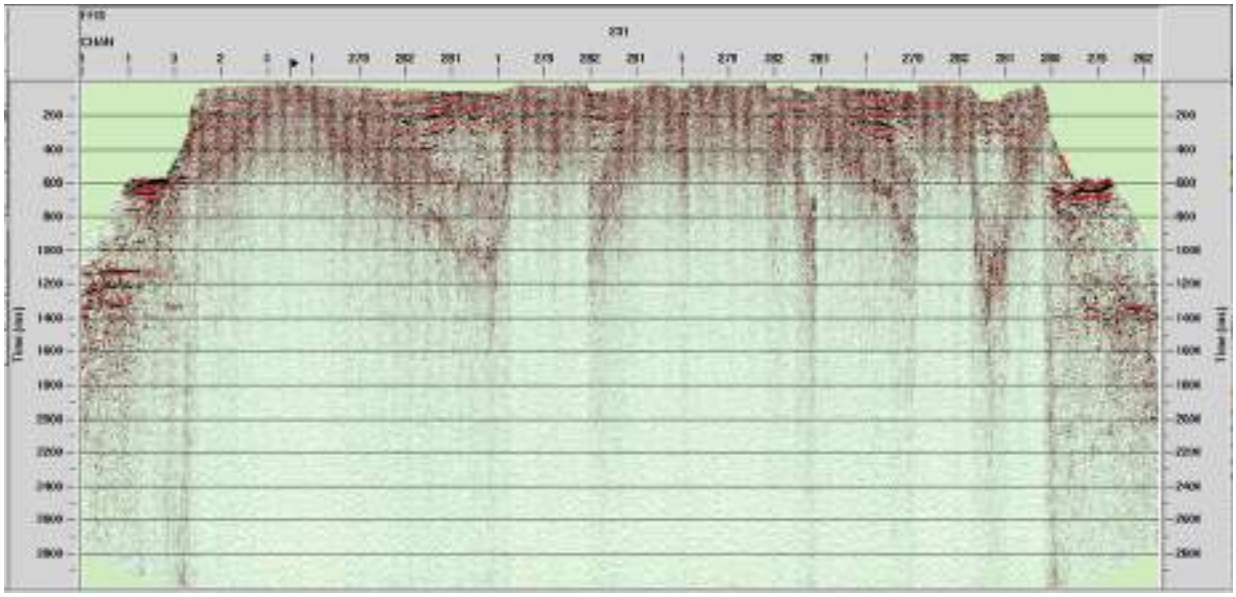

Figure 14: Brute stack with stretch muting 150%.

3.8. Automatic Gain Control (AGC)

Automatic Gain Control (AGC) automatically modifies the gain applied to seismic trace samples according to their amplitude within a defined time window. The duration of the AGC operator sets the length of this window used for gain computation. As the window slides along the trace, one sample at a time, a scaling factor is calculated at each position. This factor is usually the reciprocal of the mean, median, or root mean square (RMS) amplitude within the window, and it is applied to the sample located at the start, centre, or end of the window, depending on the selected configuration.

At the trace boundaries, where the available data is shorter than the specified operator length, the window size is adjusted to use as much data as possible. It increases incrementally at the beginning of the trace until reaching the full operator length, remains constant through the middle section, and then decreases as it nears the end of the trace.

Modes of Application:

- **Apply:** Calculates and applies AGC scaling factors to the trace.
- **Apply and Save:** Applies AGC and stores the scaling factors in the trace headers for potential inverse scaling later.
- **Remove AGC:** Reverses the AGC process by applying the inverse of the previously saved scaling factors, either from the current workflow or a prior run.
- **Output Scalar Traces:** Outputs the calculated scaling factors as separate traces.

The performance of multi-channel filters, such as frequency-wavenumber (F-K) and Radon transforms, is often enhanced when the input data is amplitude-balanced. AGC provides a straightforward and effective means of achieving this balance. However, it should be noted that AGC alters the true amplitude information of the data. To recover the original amplitude characteristics after filtering, the AGC process can be reversed using the saved scaling factors, which are then removed from the trace headers to optimise storage. To prevent excessive amplification of very weak or strong signal zones, the AGC gain can be constrained to a specified multiple of the median gain.

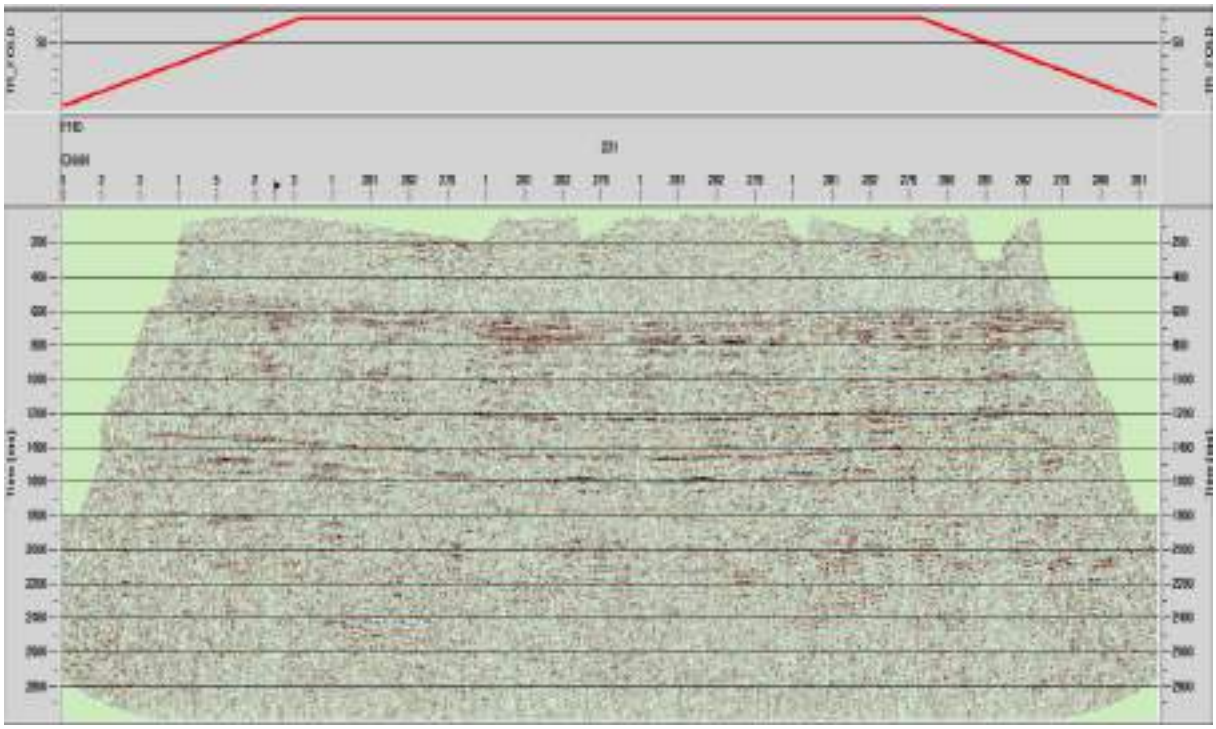

Figure 15: Brute stack after AGC, bandpass filtered with stretch muting 30%.

3.9. Bandpass Filter

A bandpass filter applies frequency-based filtering to each seismic trace, with the filtering process conducted in the frequency domain. Users can define one or more sets of bandpass filter frequencies, as well as parameters for notch filters. The available filter types include four-frequency Ormsby or Butterworth filters, which can be implemented as either zero-phase or minimum-phase filters.

This procedure supports three main approaches to bandpass filtering:

1. **Single Bandpass Filter:** A single filter is uniformly applied to all traces throughout the entire record. For the Ormsby filter, only the four corner frequencies are required, while the Butterworth filter requires a single set of frequency and slope parameters.
2. **Time-Variant Filter:** This option enables the application of filters that change over time. The user specifies the filter parameters, and the first filter is applied from the start of the trace to the end of the first window. A linear taper is then used to transition between filters across overlapping windows, ensuring smooth interpolation and minimising artefacts. The final filter remains constant from the last window to the end of the record. It is important to avoid adjacent, non-overlapping windows, as this can prevent proper interpolation and introduce processing artefacts.
3. **Time- and Spatially-Variant Filter:** This method allows for the application of time-varying filters that also change spatially along the seismic line, providing greater flexibility in adapting to varying data characteristics.

Implementation Details: The user can specify the percentage of each input trace to be zero-padded for Fast Fourier Transform (FFT) processing. In addition to the bandpass filter, a notch filter may be applied, with user control over the center frequency and bandwidth. The notch filter can also be automatically centered at the frequency of maximum spectral amplitude within a defined range, using an automatic search function. Each filter is defined by a set of four integers, separated by dashes.

The values indicate, in sequence, the 0% and 100% points of the low-cut ramp and the 100% and 0% points of the high-cut ramp (in Hz) for the Ormsby filter, as well as the -3dB low-frequency, low-slope and 3dB high-frequency, high-slope points for the Butterworth filter. In the frequency domain, the Ormsby filter ramps are shaped using cosine tapers (Hanning windows). The ramps for the Butterworth filter are generated by:

$$\frac{1}{\sqrt{1 + \left(\frac{F}{FMID}\right)^{2P}}}$$

Where:

FMID is the center frequency of the pass band
P is computed for the lower and upper slopes to get the correct dB/octave roll off.

Table 2: Bandpass filter frequency.

F1 (Hz)	F2 (Hz)	F3 (Hz)	F4 (Hz)
8	12.5	40	50

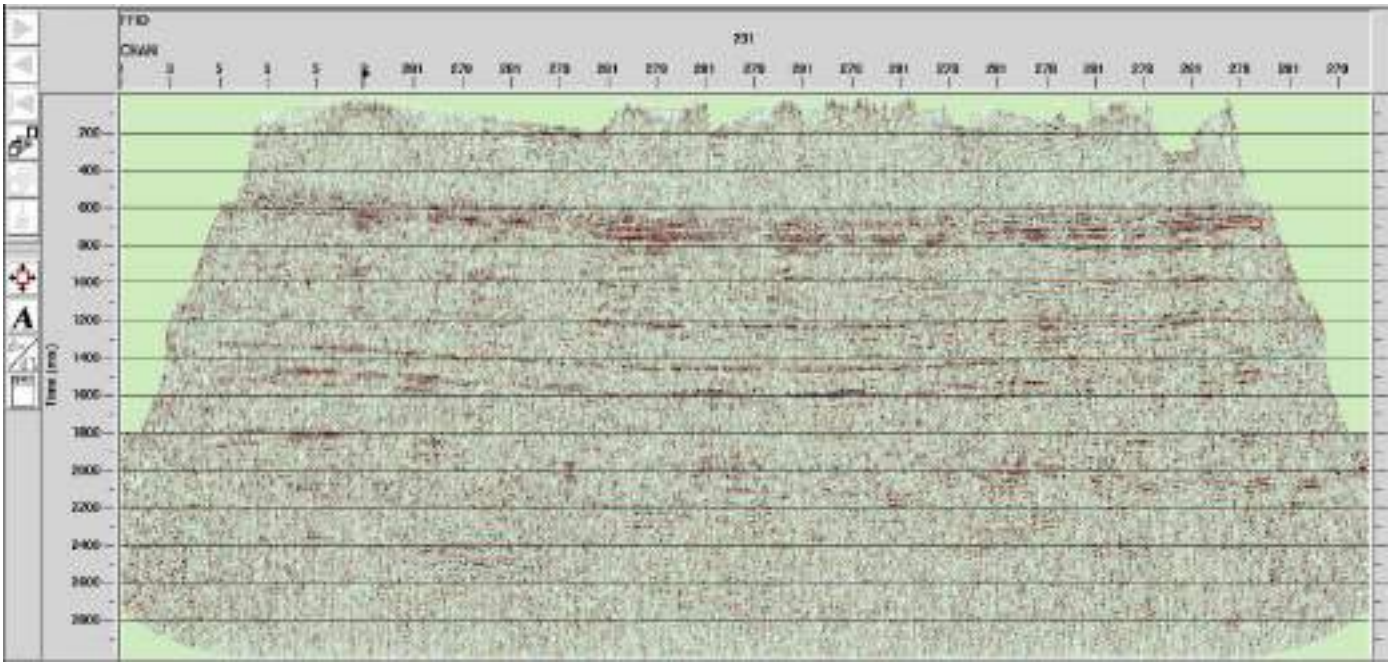

Figure 16: Brute stack after AGC, bandpass filtered with stretch muting 30%.

3.10. Frequency Analysis

As the sample rate ($dt = 2\ ms$), the Nyquist Frequency is;

$$f_{Nyquist} = \frac{1}{2 \times \Delta t} = 250\ Hz$$

Where:
Δt is sample rate in milliseconds

The frequency analysis for high-side frequency has been performed for the below windows

Window 1	Window 2	Window 3	Window 4
45 - 50 – 60 - 65	**55 – 60 – 70 – 75**	**65 – 70 – 85 – 100**	**75 – 80 – 100 - 105**

In the panel (d) the signal is weak while the last panel display the original shot gather.

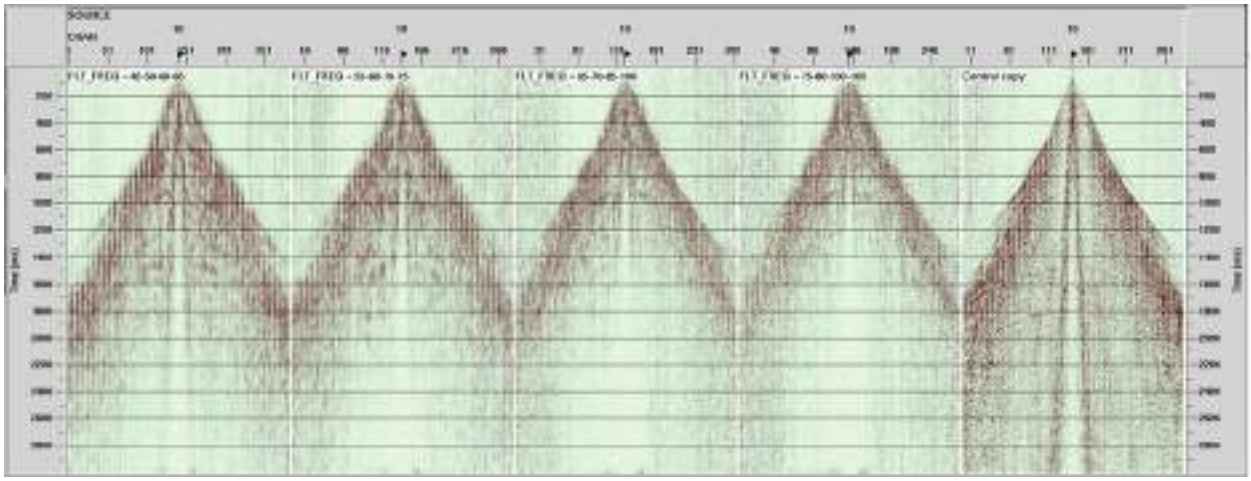

Figure 17: Frequency analysis of data.

The frequency analysis for low-side frequency has been performed for the below windows

Window 1	Window 2	Window 3	Window 4
5 – 6 – 7 -8	6 -7 – 8 – 9	7 – 8 -10 - 12	9 -10 – 12 - 14

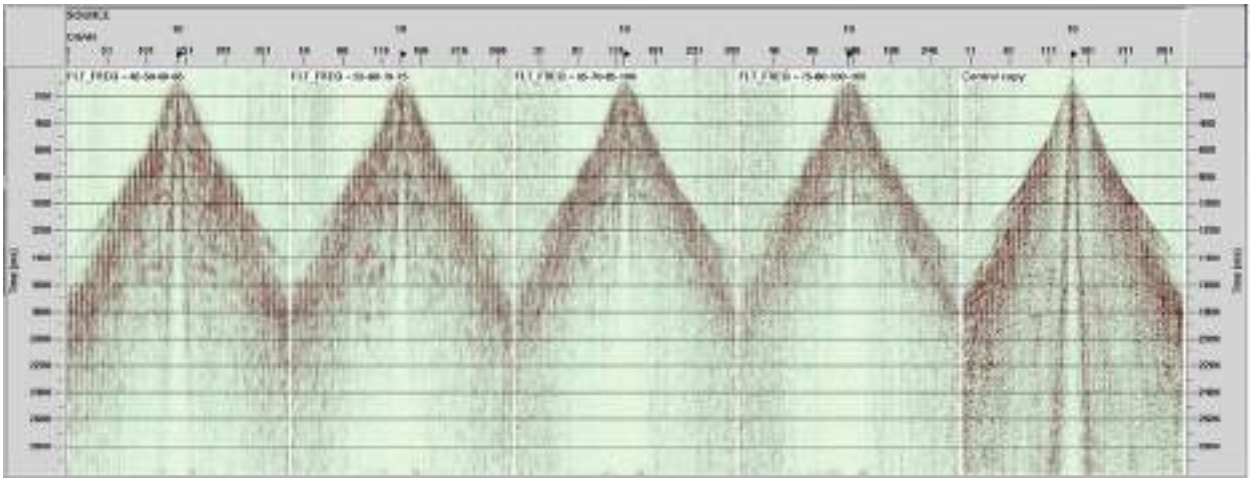

Figure 18: Frequency analysis of data.

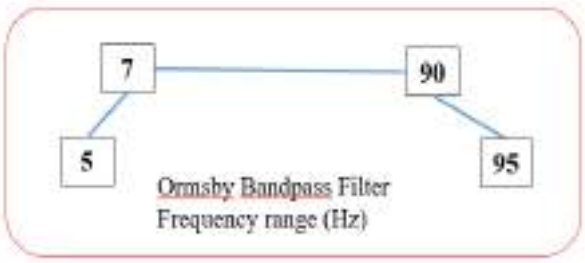

Figure 22: Ormsby **bandpass** filter entry frequencies determined for the data.

Also, from SPS file the frequency of Sweep of vibroseis is between 8-95 Hz.

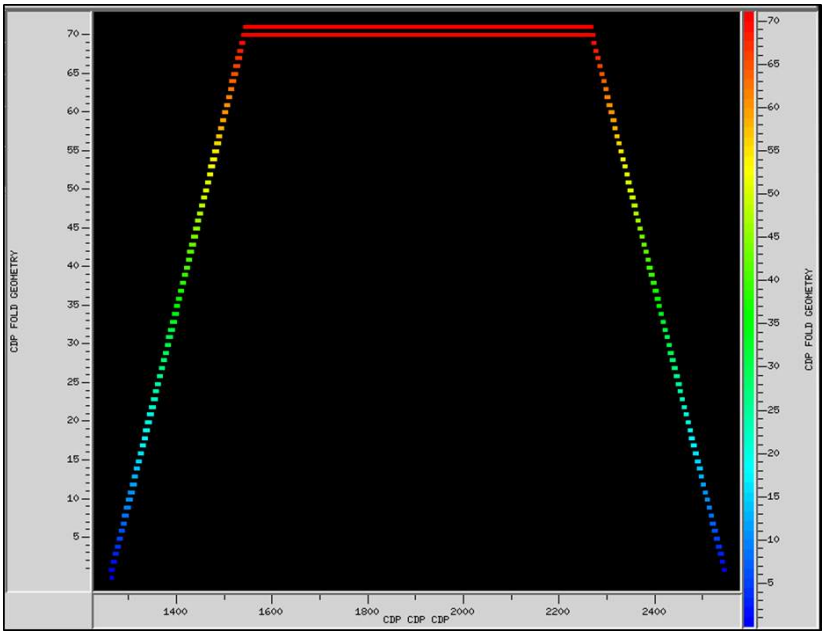

Figure 19: CDP fold coverage of data.

3.11. Fold Coverage

You should here define fold coverage and then show the CDP fold coverage of your data.

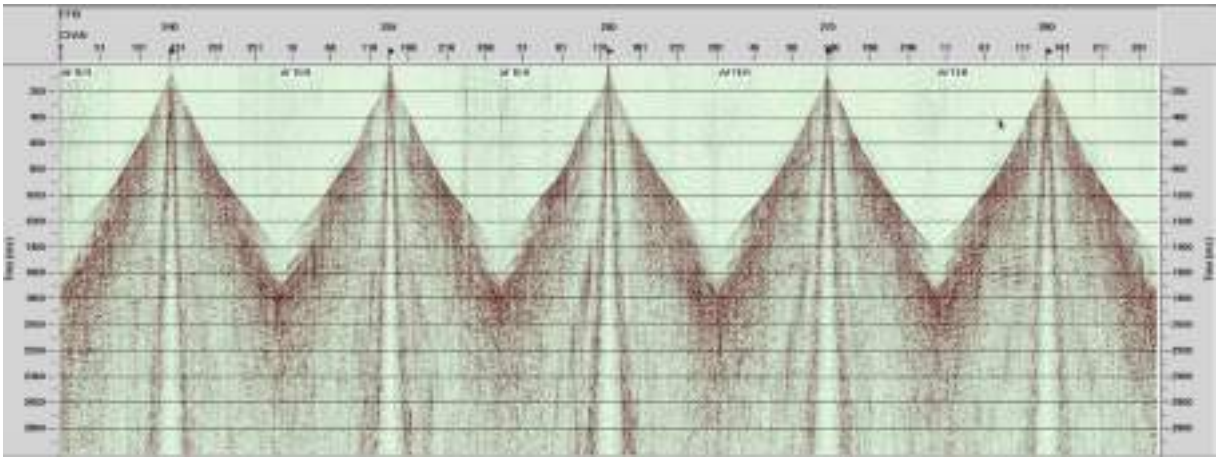

Figure 20: The selected shot gathers after applying SCA .

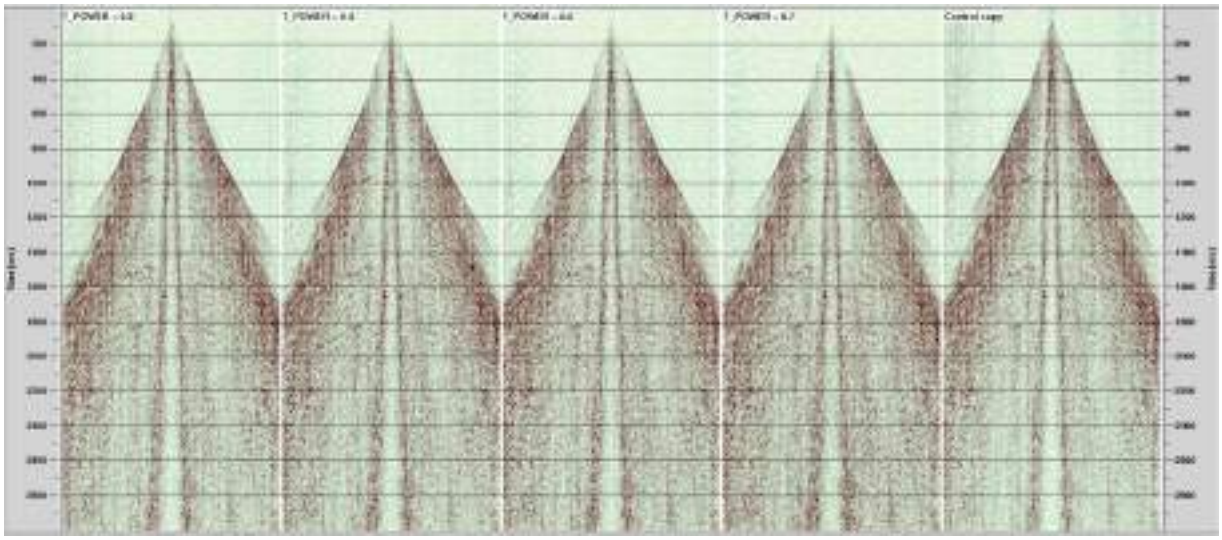

Figure 21: TAR testing best parameter.

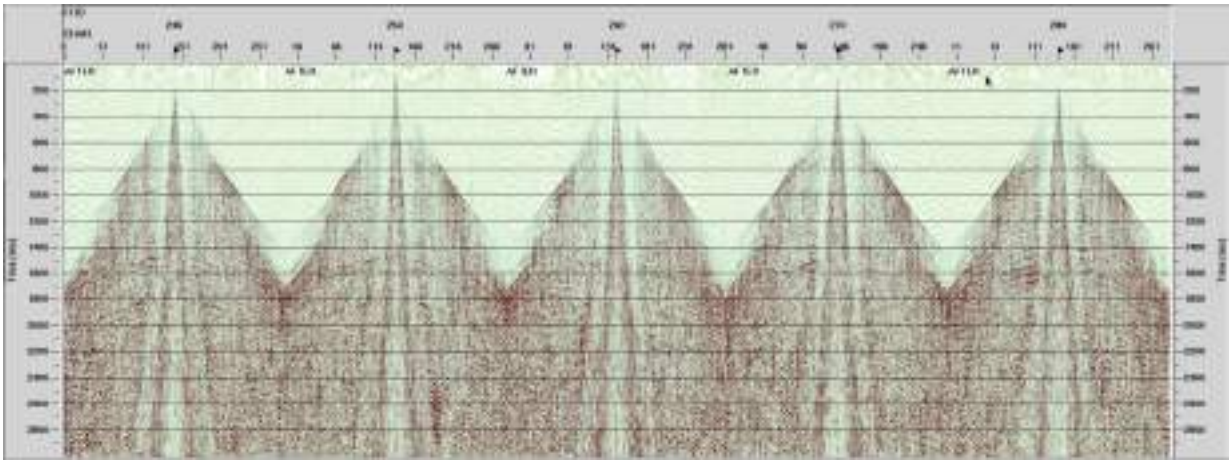

Figure 22: After removing Air wave, and Ground rolls on the gathers.

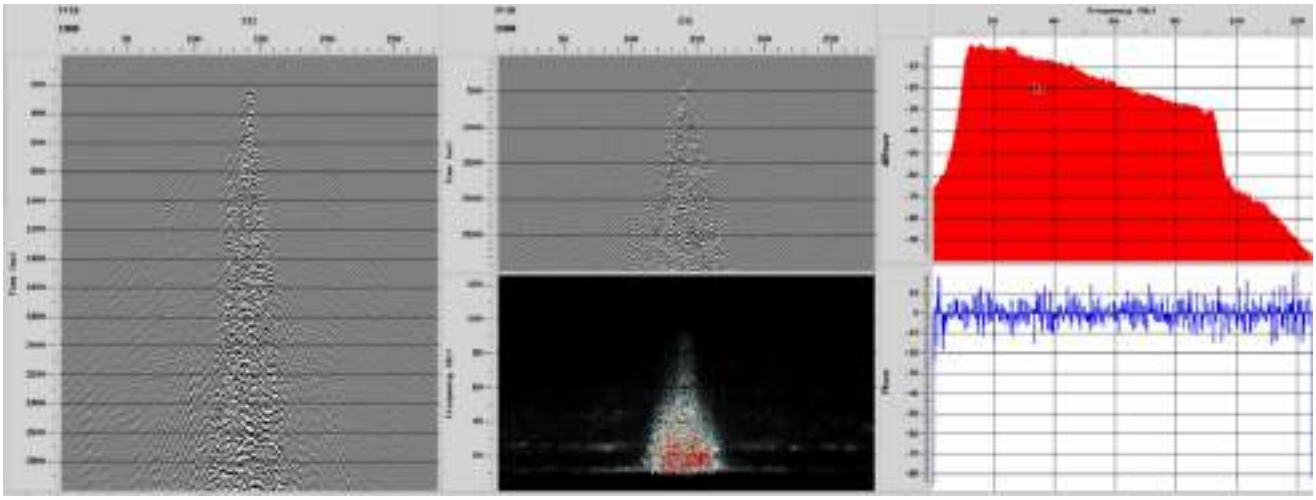

Figure 23: TAR Spectral analysis.

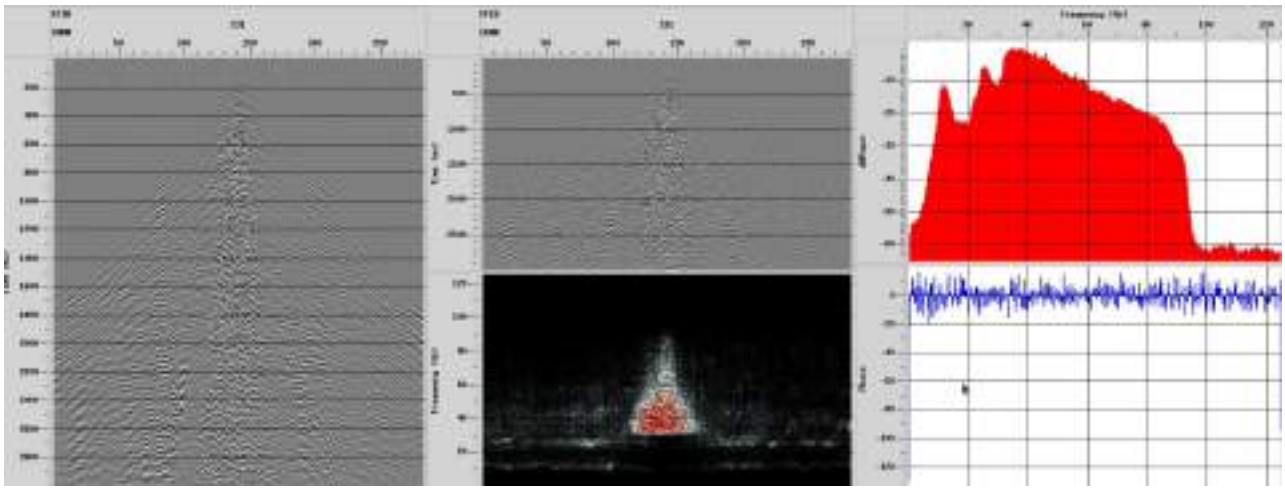

Figure 24: Spectral Analysis after reducing Air-wave, and ground roll.

4. Discussion

This study examined how to improve subsurface imaging using multiple seismic processing stages. The quality of the shot collection has an impact on the processing flow since each step serves to rectify or remove noise from the recorded data. Because of the disposition reflector, the final processing stage still does not provide the best image. Nevertheless, a better view is

provided by the seismic cross-section following the migration. By using the most effective geophysical techniques for geothermal resource development and monitoring, an understanding of seismic technologies and their applications results in better decisions. Seismic methods have been identified as an instrumental geophysical approach for assessing a geothermal prospect's potential for geothermal resources, where the techniques are useful in mapping the geological and lithological structure from interpreted velocity models, and evaluating the geothermal parameter, including the location of the heat source, suitable reservoir, and permeability by targeting potentially productive wells.

5. Conclusion

The quality of seismic products and solutions available today has advanced significantly compared to just a few years ago. Despite this progress, the rapid pace of technological development continues to present challenges in seismic data processing. In southern Iraq, 2D seismic data were collected in areas characterised by relatively flat structures, but the data were heavily affected by strong noise. The dataset contains substantial amounts of both coherent and random noise. To address this, we implemented a variety of advanced noise attenuation modules on low-fold data. We evaluated the performance of current modules and filters within our processing system to suppress noise, enhance the signal-to-noise ratio (SNR), and improve the overall quality of seismic images. The application of these noise attenuation techniques resulted in notable improvements, including enhanced frequency content, better resolution, and a higher SNR. These methods effectively reduced both random and coherent noise while preserving the integrity of the seismic signal. The resulting improvements in seismic image quality are expected to benefit subsequent processing steps and ultimately aid in more accurate interpretation.

References

Al-Heety, A. J. R., & Thabit, H. A. (2022). Random and coherent noise attenuation for 2D land seismic reflection line acquired in Iraq. NRIAG Journal of Astronomy and Geophysics, 11(1), 337–354. https://doi.org/10.1080/20909977.2022.2118982.

Al-Heety, A.J. and Thabit, H.A., 2019. Random and Coherence Noise Attenuation Complete Sequence for 2-D Land Seismic Data Acquired in Iraq. arXiv preprint arXiv:1904.10022.

Canales, L. L. (1984). Random noise reduction. SEG Technical Program Expanded Abstracts, 525-527.

Chen, Y., & Ma, J. (2014). Seismic data denoising and reconstruction using double-sparsity dictionary learning. Geophysics, 79(5), V81-V91.

Kearey, P., Brooks, M., & Hill, I. (2013). An Introduction to Geophysical Exploration (4th ed.). Wiley-Blackwell.

Perz, M., Henley, D., & Bertram, M. (2005). Time-variant spectral whitening. CSEG Recorder, 30(1), 5-13.

Rose, J. 2013. Processing and Interpretation of Vibroseismic Data from Ekstroem Ice Shelf. Antarctica 2011 (Doctoral dissertation, University of Bremen).

SEG wiki source SEG-Y Poland 2019.

Seismic Methods in Geotechnical Applications. Guideline Geo, 12 Oct. 2023, www.guidelinegeo.com/seismic-methods/.

Sheriff, R.E and Geldart, L.P, 1995. Exploration seismology, Cambridge University Press.

Stewart, R. R. (1984). Ground roll: Suppression and use. Geophysics, 49(9), 1384-1392.

Ulrych, T. J., Sacchi, M. D., & Woodbury, A. (1995). A Bayes tour of inversion: A tutorial. Geophysics, 60(6), 1941-1952.
Yilmaz O, Edited by Stephen M. Doherty, (1987) “Seismic data processing”, Society of Exploration Geophysicists (SEG) Investigations in Geophysics No. (2). Yilmaz, Ö., 2001. Seismic data analysis: Processing, inversion, and interpretation of seismic data. Society of exploration geophysicists. doi:10.1190/1. 9781560801580.